Finite Element Analysis of Electric Fracture Properties in Modified Small Punch Testing of Piezoceramic Plates

doi: 10.1063/1.1682693

Finite element analysis of electric fracture properties in modified small punch testing of piezoceramic plates

Y. Magara, F. Narita, Y. Shindo,[a] and M. Karaiwa
Department of Materials Processing, Graduate School of Engineering, Tohoku University, Aoba-yama 02, Sendai 980-8579, Japan

(Received 13 October 2003; accepted 20 January 2004)

The fracture behavior of a piezoelectric ceramic under applied electric fields has been the subject of recent studies. We have used finite element analysis to study experiments with the modified small punch (MSP) technique. Nonlinear three-dimensional finite element analysis was employed to calculate the MSP energy and maximum strain energy density. The effects of an applied electric field, 180° and 90° domain switching on the MSP energy, and maximum strain energy density are discussed, and the model predictions are compared with the results of the experiments. The polarization switching zones corresponding to combined mechanical and electrical loads are also obtained. © *2004 American Institute of Physics.* [DOI: 10.1063/1.1682693]

I. INTRODUCTION

$Pb(Zr,Ti)O_3$ (PZT) is widely used in piezoelectric devices, e.g., transducers, filters, sensors, and actuators. The high mechanical stresses and intense electric fields in the PZT ceramic may cause microcracks to develop which eventually lead to failure of the device. The fracture behavior of PZT under mechanical and electrical loads has been the subject of recent studies.[1,2] The single-edge precracked beam tests were performed on a commercial PZT ceramic, and these tests were simulated numerically with the finite element method.[3] Indentation fracture tests were also made on the PZT ceramics to estimate the fracture toughness, and a three-dimensional (3D) finite element analysis was employed to calculate the energy release rate and stress intensity factor.[4] The crack growth in a ferroelectric barium titanate ceramic was investigated under applied electric fields up to four times the coercive field strength by using the Vickers indentation technique, and the change in crack length and fracture toughness was discussed in connection with the influence of polarization switching on the crack generating stresses.[5] The Vickers indentation technique was also used to study the fracture behavior of poled ferroelectrics.[6] Direct observations of domain switching were made, which suggest that switching induced by the indenter itself plays an important role in determining the apparent fracture toughness.

In a series of articles, a model was developed to simulate the observed nonlinearities in material behavior.[7,8] The ceramics were considered as an aggregate of many grains which were modeled as single domain with switching. Investigated in Ref. 9 was the fracture toughness variation due to small-scale domain switching near the tip of a conducting crack. The shape of the switching zone around a crack tip was predicted by a work energy-based switching criterion. Hayashi *et al.*[10] investigated the displacement and polarization switching properties of piezoelectric laminated actuators theoretically, numerically, and experimentally. Shindo *et al.*[11] examined the effects of applied voltage and polarization switching on the electroelastic field concentrations ahead of electrodes in multilayer piezoelectric actuators in a combined experimental and numerical investigation.

In the present article, fracture behavior of a piezoelectric ceramic under an applied electric field is discussed using the modified small punch (MSP) test technique. The purpose of the present article is also to present a model for such a MSP test. This is done with a nonlinear finite element analysis of the whole apparatus, which includes the punch, the piezoelectric plate specimen, and the specimen holder. To carry out the analysis, a polarization switching model is assumed for the specimen material. The MSP energy and maximum strain energy density are calculated to qualitatively account for the effect of electric field on fracture initiation load obtained by the MSP test.

II. EXPERIMENTAL PROCEDURE

Commercially supplied P-7 (Murata Manufacturing Co., Ltd., Japan) piezoelectric ceramic was selected for the experiment. The material properties are listed in Table I. The coercive electric field E_c is 0.8 MV/m. At least 32 small, thin piezoceramic plate specimens of $10\times10\times0.5$ mm used for the MSP tests were sliced. Poling was done along the axis of the 0.5 mm dimension, and silver electrodes were coated on the two 10 mm$\times$10 mm surfaces.

All MSP tests were conducted using a screw-driven test machine. To generate electric fields, a power supply for voltages up to 1.25 kV/dc was used to apply positive and negative electric fields of 0.2, 0.4, 0.8, and 1.0 MV/m. Loads which caused fracture were measured for each set of specimens for various electric fields. For 0, ±0.4, ±0.8, and ±1.0 MV/m, four or five tests were performed.

III. BASIC EQUATIONS AND PREDICTION OF POLARIZATION SWITCHING

In this section, the governing field equations for a ferroelectric will be summarized.

[a]Electronic mail: shindo@material.tohoku.ac.jp

TABLE I. Material properties of the P-7 piezoelectric ceramic.

Elastic stiffnesses ($\times 10^{10}$ N/m^2)					Piezoelectric coefficients ($\times 10^{-12}$ m/V)			Dielectric constants ($\times 10^{-10}$ C/Vm)	
c_{11}	c_{33}	c_{44}	c_{12}	c_{13}	d_{31}	d_{33}	d_{15}	ε_{11}	ε_{33}
13.0	11.9	2.5	8.3	8.3	−207	410	550	171	186

Newton's and Gauss' laws give

$$\sigma_{ji,j}=0, \tag{1}$$

$$D_{i,i}=0, \tag{2}$$

where σ_{ij} and D_i are the stress and electric displacement, and a comma followed by an index denotes partial differentiation with respect to a space coordinate $x_i(i=1,2,3)$. We have employed Cartesian tensor notation and the summation convention for repeated tensor indices. Quasistatic and small strain conditions are

$$E_i=-\phi_{,i}, \tag{3}$$

$$\varepsilon_{ij}=\frac{1}{2}(u_{j,i}+u_{i,j}), \tag{4}$$

where E_i and ϕ are the electric field and electric potential, and ε_{ij} and u_i are the strain and displacement. In a ferroelectric, domain-wall motion within each grain leads to a change in the remanent strain ε_{ij}^r and remanent polarization P_i^r. The total strain and electric displacement are given by

$$\varepsilon_{ij}=\varepsilon_{ij}^{\ell}+\varepsilon_{ij}^{r}, \tag{5}$$

$$D_i=D_i^{\ell}+P_i^{\mathrm{r}}, \tag{6}$$

where the superscript ℓ refers to linear and

$$\varepsilon_{ij}^{\ell}=s_{ijkl}\sigma_{kl}+d_{kij}E_k, \tag{7}$$

$$D_i^{\ell}=d_{ikl}\sigma_{kl}+\varepsilon_{ik}^{T}E_k. \tag{8}$$

In Eqs. (7) and (8), s_{ijkl}, d_{kij} and ε_{ik}^T are the elastic compliance, direct piezoelectric constant, and dielectric permittivity at constant stress, which satisfy the following symmetry relations:

$$s_{ijkl}=s_{jikl}=s_{ijlk}=s_{jilk}=s_{klij}, \quad d_{kij}=d_{kji}, \quad \varepsilon_{ik}^T=\varepsilon_{ki}^T. \tag{9}$$

The direction of spontaneous polarization P^s of each grain can change by 90° or 180° for ferroelectric switching induced by a sufficiently large electric field. The 90° ferroelastic domain switching is induced by a sufficiently large stress field. Figure 1 shows the schematics of polarization switching for different types of external loading. The criterion states that a polarization switches when the electrical and mechanical work exceeds a critical value[7]

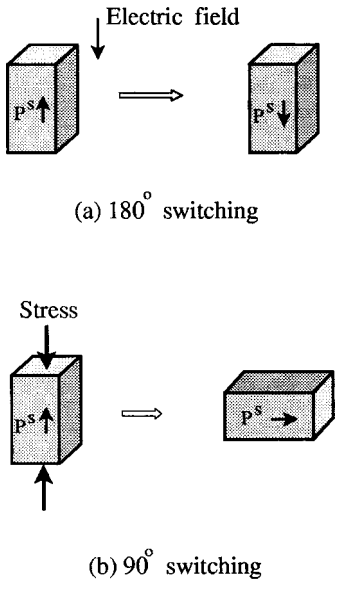

FIG. 1. Polarization switching induced by electrical and mechanical loads.

$$\sigma_{ij}\Delta\varepsilon_{ij}+E_i\Delta P_i \geqslant 2P^sE_c, \tag{10}$$

where $\Delta\varepsilon_{ij}$ and ΔP_i are the changes in the spontaneous strain and spontaneous polarization during switching, respectively, and E_c is the coercive electric field. The values of $\Delta\varepsilon_{ij}$ and ΔP_i are given in Appendix A.

While each grain obeys the constitutive relations (7) and (8), the direct piezoelectric constant in the constitutive relations depends on the orientation of the polarization vector in the ceramic. The components of the piezoelectricity tensor during switching are

$$d'_{ikl}=\Big\{ d_{33}n_in_kn_l+d_{31}(n_i\delta_{il}-n_in_kn_l) + \frac{1}{2}d_{15}(\delta_{ik}n_l-2n_in_kn_l+\delta_{il}n_k)\Big\}, \tag{11}$$

where n_i is the unit vector in the poling direction, δ_{ij} is the Kroneker delta, and $d_{33}=d_{333}$, $d_{31}=d_{311}$, and $d_{15}=2d_{131}$ are the direct piezoelectric constants when the piezoelectric ceramic is completely poled in the x_3 direction. The primed quantities denote the piezoelectric constants associated with the original coordinate system during the polarization switching. σ_{ij} and D_i^{ℓ} during polarization switching are related to ε_{ij}^{ℓ} and E_k by

$$\sigma_{ij}=c_{ijkl}\varepsilon_{kl}^{\ell}-e'_{kij}E_k, \tag{12}$$

$$D_i^{\ell}=e'_{ikl}\varepsilon_{kl}^{\ell}+\varepsilon_{ik}E_k, \tag{13}$$

where c_{ijkl} and e'_{ikl} are the elastic and piezoelectric constants, ε_{ik} is the dielectric permittivity at constant strain, and

$$c_{ijkl}=c_{jikl}=c_{ijlk}=c_{jilk}=c_{klij}, \quad e'_{kij}=e'_{kji}, \quad \varepsilon_{ik}=\varepsilon_{ki}. \tag{14}$$

For the 180° switching, the coercive field is obtained as

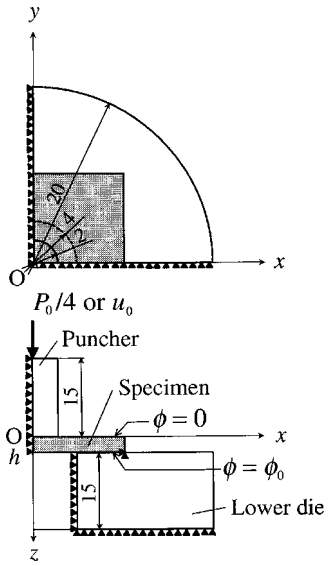

FIG. 2. Finite element model of the MSP test.

$$E_3 = -E_c, \tag{15}$$

which is not affected by the applied stress. However, according to the criterion in Ref. 12, the coercive field for 180° switching is

$$E_3 = -\frac{E_c}{1-(2d_{33}/P^s)\sigma_{33}}. \tag{16}$$

It is noted that the second term in the denominator includes the normal stress effect as a result of piezoelectricity, and the coercive field increases or decreases depending on the magnitude and direction of the stress σ_{33}.

VI. FINITE ELEMENT ANALYSIS

We performed 3D finite element calculations to determine the MSP energy and maximum strain energy density for the PZT specimens. A rectangular Cartesian coordinate system (x,y,z) is used with the z axis coinciding with the poling direction. The analytical model is shown in Fig. 2. A mechanical load was produced by the application of either a prescribed force P_0 or a prescribed displacement u_0 along the z direction. For electrical loads, a negative or positive electric potential ϕ_0 was added on the surface, $z=h$. The surface $z=0$ is grounded. We used the commercial finite element code ANSYS. Eight-node 3D space solid was used in the analysis. The contact between the specimen and the lower die was modeled using contact elements. Young's modulus and Poisson's ratio of the puncher and lower die are taken to be $E=206$ GPa and $\nu=0.3$. Because of the double symmetry of the body and loading, only one-quarter of the body was modeled. The total number of nodes and elements in the finite element calculations were 6445 and 15 057, respectively. Each 3D finite element consists of about 10 000 grains.

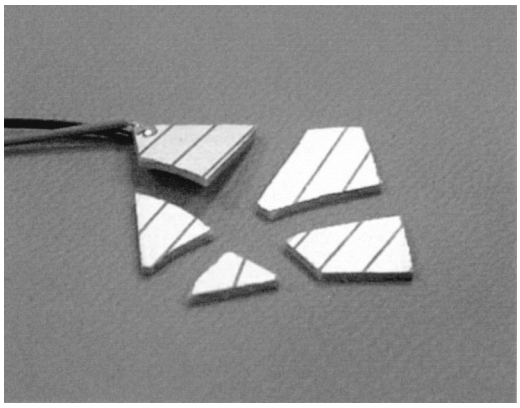

FIG. 3. Fracture appearance of MSP specimen.

The polarization of each grain initially aligns as closely as possible with the z direction. The constitutive Eqs. (12) and (13) for PZT poled in the z direction are found in Appendix B. The polarization switching is defined for each element in a material. Boundary loads are applied, and the electroelastic fields of each element are computed from the finite element analysis. The switching criterion of Eq. (10) is checked for every element to see if switching will occur. After all possible polarization switches have occurred, the piezoelectricity tensor of each element is rotated to the polarization direction. The piezoelectric constant e'_{ikl} of each element is given in Appendix C. The electroelastic fields are recalculated, and the process is repeated until the solution converges. The macroscopic response of the material is determined by the finite element model, which is an aggregate of elements. The spontaneous polarization P^s and strain γ^s are assigned representative values of 0.3 C/m^2 and 0.004, respectively.

V. RESULTS AND DISCUSSION

Figure 3 shows the fracture appearance of piezoelectric ceramic P-7. All specimens failed in a brittle manner. Table II shows the average fracture initiation loads P_c and the statistically determined standard deviations under different electric fields E_0 obtained from the experiment. At low electric field levels, positive electric fields increase the fracture initiation load. A decrease in the fracture initiation load at $E_0 = 1.0$ MV/m is considered to occur because of dielectric

TABLE II. Average fracture initiation loads and statistical standard deviations under electric fields for MSP specimens.

	P_c (N)	
E_0 (MV/m)	Average	Standard deviation
−1.0	17.7	5.0
−0.8	15.5	2.8
−0.4	13.9	1.6
−0.2	11.9	···
0.0	13.7	0.49
+0.2	15.0	···
+0.4	16.6	2.0
+0.8	17.5	0.35
+1.0	4.79	1.0

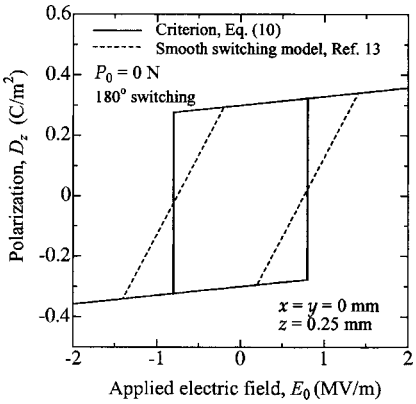

FIG. 4. Polarization vs applied electric field for $P_0=0$ N.

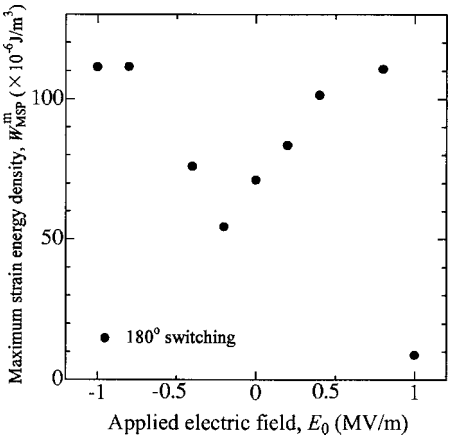

FIG. 6. Maximum strain energy density vs applied electric field.

breakdown and irreversible damage of the PZT. When the electric-field level in the negative direction reaches coercive field, $E_0=-0.8$ MV/m, the direction of polarization of the stress-free sample switches. At $E_0=-1.0$ MV/m, the polarization has reversed and is now aligned with the negative electric field. Also, the effective coercive field under applied stress changes as a function of mechanical load. The behavior of the fracture initiation load for approximately $E_0=-0.4$ MV/m leading to $E_0=-1.0$ MV/m is expected to be very complicated because of all of these phenomena.

Figure 4 shows the polarization D_z at $x=y=0$ mm, $z=h/2=0.25$ mm versus electric field E_z for $P_0=0$ N. The model was used to predict macroscopic nonlinear response involving 180° switching, and simulations were carried out with the assumption that the value of saturation polarization is 0.3 C/m^2. The hysteresis loop for $P_0=0$ N shows that switching commences when $E_0=\pm 0.8$ MV/m and changes rapidly as the electric-field magnitude increases. The curves generated by the model are also compared with a smooth switching model[13] (see Appendix D). When the smooth switching modeling type is used, the shape of polarization–electric-field curve is changed. However, the strain–electric field curves for the MSP specimens are almost the same for these two models (not shown).

Shindo *et al.*[14] used the small punch (SP) test to characterize the elastic–plastic fracture toughness J_{IC} of structural alloys and weldments for superconducting magnets, and assessed correlation between SP energy and J_{IC}. Fracture properties measured using this miniature specimen testing approach have been shown to reasonably accurate for a wide range of metals, but have yet to be explored for piezoelectric ceramics. Figure 5 presents the critical MSP energy E^c_{MSP} including 180° and 90° switching effects (open triangle) for various electric fields E_0. The load–displacement curves were drawn up to the average fracture initiation load P_c using the finite element method, and the E^c_{MSP} was calculated from the area under the curve (energy to failure). It is interesting to note that the MSP energies for $E_0=+0.8$ MV/m and $E_0=-0.8$ MV/m have very nearly the same values. A similar phenomenon was observed for E^c_{MSP} without 90° switching effect (solid circle), and the 90° switching has no effect on the critical MSP energy. Figure 6 shows the maximum strain energy density W_{MSP} versus E_0. The W_{MSP} as a function of applied load is computed via finite element analysis without 90° switching effect. The W^m_{MSP} occurs at the observed crack initiation location.

Figure 7 shows the MSP energy E_{MSP} of the finite element solutions without the 90° switching effect under an average fracture initiation load for zero electric field $P_0=13.7$ N and different electric fields E_0, where the result has been normalized by the MSP energy E_{MSP0} for E_0

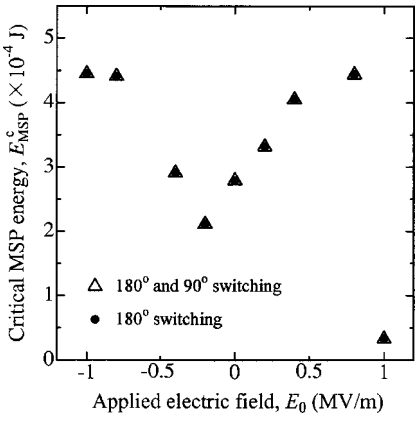

FIG. 5. Critical MSP energy vs applied electric field.

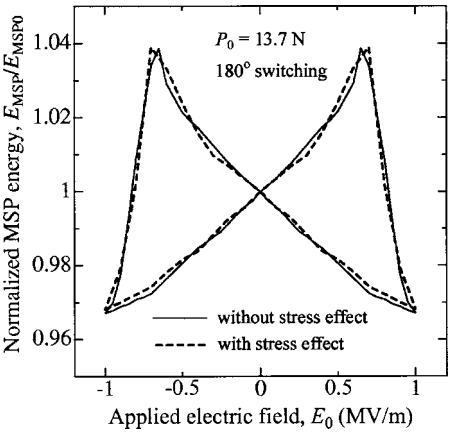

FIG. 7. MSP energy under various electric fields for applied force.

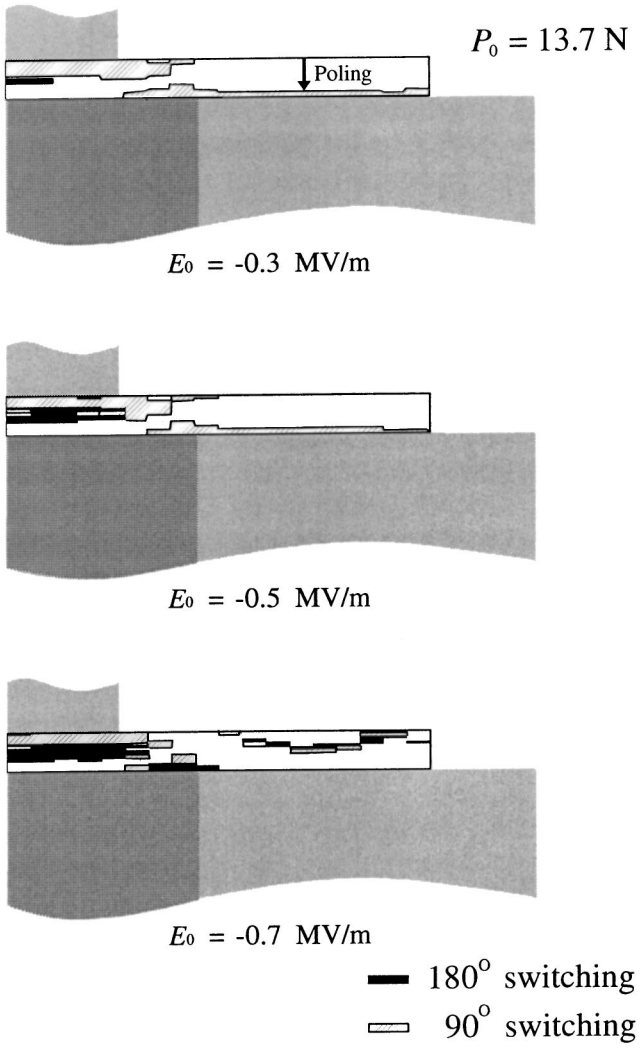

FIG. 8. Polarization switching zone induced by applied force and electric field.

$=0$ MV/m. Also shown are the prediction with stress effect for the MSP specimen by Eq. (16). The curve rises at first when the electric field E_0 is reduced starting at zero. As the electric field E_0 continues to be reduced, polarization switching commences at approximately $E_0=-0.5$ MV/m and since the remanent polarization is now diminishing, the MSP energy falls. The electric field in the z direction is now increased again toward 1.0 MV/m. The results show that switching recommences at approximately $E_0=0.5$ MV/m to eliminate the existing negative remanent polarization. This is completed by the time the field reaches approximately 0.7 MV/m. As the field is cycled between approximately -1.0 MV/m and 1.0 MV/m, the hysteresis curve is reproduced. In addition, it is noted that the results using either Eqs. (15) or (16) are almost the same for the thin piezoelectric plates. Figure 8 shows the 180° and 90° switching zones of the specimen under $P_0=13.7$ N and $E_0=-0.3$, -0.5, and -0.7 MV/m. The size of the switching zone increases with increasing negative electric field.

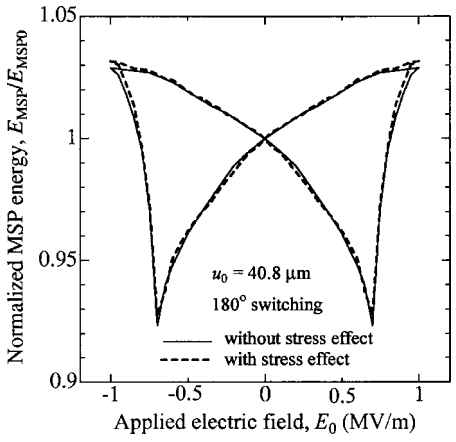

FIG. 9. MSP energy under various electric fields for applied displacement.

Using a reaction at $x=0$, $z=0$ for $P_0=13.7$ N and $E_0=0$ MV/m, the applied displacement, $u_0=40.8\,\mu$m, was obtained. Figure 9 shows the normalized MSP energy E_{MSP}/E_{MSP0} of the finite element solutions without the 90° switching effect under a constant displacement $u_0=40.8\,\mu$m and different electric fields E_0. For a given displacement, the MSP energy decreases at first when the electric field E_0 is reduced starting at zero. As the electric field E_0 continues to be reduced, a negative remanent polarization develops in the portion of the specimen and the MSP energy rises steeply. As the field is cycled between approximately -1.0 MV/m and 1.0 MV/m, the butterfly loop is repeated. The numerical results under a constant displacement are in contrast to those under an applied force. Fracture mechanism is due to the addtional stress induced by the applied electric field.

VI. CONCLUSIONS

The fracture behavior of piezoelectric ceramic P-7 was investigated under mechanical and electrical loads utilizing the MSP technique. A finite element model was developed to simulate the relation between MSP energy and applied electric field. The strain energy density was also computed. These results have four important consequences: (i) Measured fracture initiation loads and calculated maximum strain energy density are sensitive to the change in the applied electric field and polarization switching. (ii) At low electric field levels, a negative (positive) electric field introduced starting at zero increases (decreases) the computed values of MSP energy for applied load. For applied displacement, the negative (positive) electric field decreases (increases) the MSP energy, at first. (iii) The increase of the negative electric field causes the switched area to grow, and the MSP energy versus electric-field curves show the nonlinear behavior. (iv) For the piezoelectric thin plates, the 180° switching dominates the nonlinear material response, and the 90° switching can be neglected.

APPENDIX A

The values in $\Delta\varepsilon_{kl}$ and ΔP_i for 180° switching can be expressed as

$$\Delta\varepsilon_{11}=0,\quad \Delta\varepsilon_{22}=0,\quad \Delta\varepsilon_{33}=0,$$

$$\Delta\varepsilon_{12}=0,\quad \Delta\varepsilon_{23}=0,\quad \Delta\varepsilon_{31}=0, \tag{A1}$$

$$\Delta P_1=0,\quad \Delta P_2=0,\quad \Delta P_3=-2P^s. \tag{A2}$$

For 90° switching in the x_2x_3 plane, there results

$$\Delta\varepsilon_{11}=0,\quad \Delta\varepsilon_{22}=\gamma^s,\quad \Delta\varepsilon_{33}=-\gamma^s,$$

$$\Delta\varepsilon_{12}=0,\quad \Delta\varepsilon_{23}=0,\quad \Delta\varepsilon_{31}=0, \tag{A3}$$

$$\Delta P_1=0,\quad \Delta P_2=\pm P^s,\quad \Delta P_3=-P^s, \tag{A4}$$

where γ^s is the spontaneous strain. For 90° switching in the x_3x_1 plane,

$$\Delta\varepsilon_{11}=\gamma^s,\quad \Delta\varepsilon_{22}=0,\quad \Delta\varepsilon_{33}=-\gamma^s,$$

$$\Delta\varepsilon_{12}=0,\quad \Delta\varepsilon_{23}=0,\quad \Delta\varepsilon_{31}=0, \tag{A5}$$

$$\Delta P_1=\pm P^s,\quad \Delta P_2=0,\quad \Delta P_3=-P^s. \tag{A6}$$

APPENDIX B

For piezoceramics which exhibit the symmetry of a hexagonal crystal of class 6 mm with respect to the principal x, y, and z axes, the constitutive relations can be written in the following form:

$$\begin{Bmatrix}\sigma_{xx}\\ \sigma_{yy}\\ \sigma_{zz}\\ \sigma_{yz}\\ \sigma_{zx}\\ \sigma_{xy}\end{Bmatrix}=\begin{bmatrix}c_{11}&c_{12}&c_{13}&0&0&0\\ c_{12}&c_{11}&c_{13}&0&0&0\\ c_{13}&c_{13}&c_{33}&0&0&0\\ 0&0&0&c_{44}&0&0\\ 0&0&0&0&c_{44}&0\\ 0&0&0&0&0&c_{66}\end{bmatrix}\begin{Bmatrix}\varepsilon^{\ell}_{xx}\\ \varepsilon^{\ell}_{yy}\\ \varepsilon^{\ell}_{zz}\\ 2\varepsilon^{\ell}_{yz}\\ 2\varepsilon^{\ell}_{zx}\\ 2\varepsilon^{\ell}_{xy}\end{Bmatrix}-\begin{bmatrix}0&0&e'_{31}\\ 0&0&e'_{31}\\ 0&0&e'_{33}\\ 0&e'_{15}&0\\ e'_{15}&0&0\\ 0&0&0\end{bmatrix}\begin{Bmatrix}E_x\\ E_y\\ E_z\end{Bmatrix}, \tag{B1}$$

$$\begin{Bmatrix}D^{\ell}_x\\ D^{\ell}_y\\ D^{\ell}_z\end{Bmatrix}=\begin{bmatrix}0&0&0&0&e'_{15}&0\\ 0&0&0&e'_{15}&0&0\\ e'_{31}&e'_{31}&e'_{33}&0&0&0\end{bmatrix}\begin{Bmatrix}\varepsilon^{\ell}_{xx}\\ \varepsilon^{\ell}_{yy}\\ \varepsilon^{\ell}_{zz}\\ 2\varepsilon^{\ell}_{yz}\\ 2\varepsilon^{\ell}_{zx}\\ 2\varepsilon^{\ell}_{xy}\end{Bmatrix}+\begin{bmatrix}\varepsilon_{11}&0&0\\ 0&\varepsilon_{11}&0\\ 0&0&\varepsilon_{33}\end{bmatrix}\begin{Bmatrix}E_x\\ E_y\\ E_z\end{Bmatrix}, \tag{B2}$$

where

$$\left.\begin{aligned}c_{11}=c_{1111}=c_{2222},\quad c_{12}=c_{1122},\quad c_{13}=c_{1133}=c_{2233},\quad c_{33}=c_{3333}\\ c_{44}=c_{2323}=c_{3131},\quad c_{66}=c_{1212}=\frac{1}{2}(c_{11}-c_{12})\end{aligned}\right\}, \tag{B3}$$

$$\left.\begin{aligned}e'_{15}=e'_{131}=e'_{223}=d_{15}c_{44},\quad e'_{31}=e'_{311}=e'_{322}=d_{31}(c_{11}+c_{12})+d_{33}c_{13}\\ e'_{33}=e'_{333}=2d_{31}c_{13}+d_{33}c_{33}\end{aligned}\right\}. \tag{B4}$$

APPENDIX C

The piezoelectric constant e'_{ikl} is related to the elastic and direct piezoelectric constants by

$$\begin{aligned}
e'_{111}&=d'_{111}c_{11}+d'_{122}c_{12}+d'_{133}c_{13},\\
e'_{122}&=d'_{111}c_{12}+d'_{122}c_{11}+d'_{133}c_{13},\\
e'_{133}&=d'_{111}c_{13}+d'_{122}c_{13}+d'_{133}c_{33},\\
e'_{123}&=2d'_{123}c_{44},\\
e'_{131}&=2d'_{131}c_{44},\\
e'_{112}&=2d'_{112}c_{66},\\
e'_{211}&=d'_{211}c_{11}+d'_{222}c_{12}+d'_{233}c_{13},\\
e'_{222}&=d'_{211}c_{12}+d'_{222}c_{11}+d'_{233}c_{13},\\
e'_{233}&=d'_{211}c_{13}+d'_{222}c_{13}+d'_{233}c_{33},\\
e'_{223}&=2d'_{223}c_{44},\\
e'_{231}&=2d'_{231}c_{44},\\
e'_{212}&=2d'_{212}c_{66},\\
e'_{311}&=d'_{311}c_{11}+d'_{322}c_{12}+d'_{333}c_{13},\\
e'_{322}&=d'_{311}c_{12}+d'_{322}c_{11}+d'_{333}c_{13},
\end{aligned} \tag{C1}$$

$$e'_{333}=d'_{311}c_{13}+d'_{322}c_{13}+d'_{333}c_{33},$$

$$e'_{323}=2d'_{323}c_{44},$$

$$e'_{331}=2d'_{331}c_{44},$$

$$e'_{312}=2d'_{312}c_{66}.$$

APPENDIX D

In this Appendix, the smooth switching model is outlined. Kamlah and Tsakmakis[13] postulated the existence of a region of reversible behavior, such that sufficiently small changes of the electric field cause no change of the remanent polarization P_3^r. Only the normal strain ε_{33} and electric displacement D_3 were considered. For this case, the normal strain ε_{33} and electric displacement D_3 during 180° switching are

$$\varepsilon_{33}=s_{13}\sigma_{11}+s_{13}\sigma_{22}+s_{33}\sigma_{33}+d'_{33}E_3, \tag{D1}$$

$$D_3=d'_{31}\sigma_{11}+d'_{31}\sigma_{22}+d'_{33}\sigma_{33}+P_3(E_3), \tag{D2}$$

$P_3(E_3)$ is given by

$$P_3(E_3)=\begin{cases}\varepsilon_{33}^T E_3-P_{\mathrm{sat}} & 0\leqslant E_3<E_c\\ (1/c^p+\varepsilon_{33}^T)E_3-E_c/c^p & E_c\leqslant E_3<E_c+c^pP_{\mathrm{sat}},\\ \varepsilon_{33}^T E_3+P_{\mathrm{sat}} & E_c+c^pP_{\mathrm{sat}}\leqslant E_3\end{cases} \tag{D3}$$

and

$$P_3(E_3)=\begin{cases}\varepsilon_{33}^T E_3+P_{\mathrm{sat}} & -E_c+c^pP_{\mathrm{sat}}<E_3<0\\ (1/c^p+\varepsilon_{33}^T)E_3+E_c/c^p & -E_c-c^pP_{\mathrm{sat}}<E_3\leqslant -E_c+c^pP_{\mathrm{sat}},\\ \varepsilon_{33}^T E_3-P_{\mathrm{sat}} & E_3\leqslant -E_c-c^pP_{\mathrm{sat}}\end{cases} \tag{D4}$$

where P_{sat} is saturation polarization and c^p is non-negative material constant. $P_{\mathrm{sat}}=0.3\,\mathrm{C/m^2}$ and $c^p=2.0\,\mathrm{MV\,m/C}$ are used to get ε_{33} and D_3.

ACKNOWLEDGMENTS

This work was supported by the Ministry of Education, Culture, Sports, Science, and Technology of Japan under a Grant-in-Aid for Scientific Research (B) and a Grant-in-Aid for Exploratory Research.

[1] Y. Shindo, K. Watanabe, and F. Narita, Int. J. Eng. Sci. **38**, 1 (2000).
[2] F. Narita and Y. Shindo, Theoret. Appl. Fract. Mech. **36**, 73 (2001).
[3] Y. Shindo, H. Murakami, K. Horiguchi, and F. Narita, J. Am. Ceram. Soc. **85**, 1243 (2002).
[4] Y. Shindo, M. Oka, and K. Horiguchi, ASME J. Eng. Mater. Technol. **123**, 293 (2001).
[5] G. A. Schneider and V. Heyer, J. Eur. Ceram. Soc. **19**, 1299 (1999).
[6] M. J. Busche and K. J. Hsia, Scr. Mater. **44**, 207 (2001).
[7] S. C. Hwang, C. S. Lynch, and R. M. McMeeking, Acta Metall. Mater. **43**, 2073 (1995).
[8] W. Chen and C. S. Lynch, Acta Mater. **46**, 5303 (1998).
[9] R. K. N. D. Rajapakse and X. Zeng, Acta Mater. **49**, 877 (2001).
[10] K. Hayashi, Y. Shindo, and F. Narita, J. Appl. Phys. **94**, 4603 (2003).
[11] Y. Shindo, M. Yoshida, F. Narita, and K. Horiguchi, J. Mech. Phys. Solids (to be published).
[12] C. T. Sun and L. Z. Jiang, *Proceedings of the Fourth European Conference on Smart Structures and Materials*,Harrogate, UK (Institute of Physics Publishing, Bristol, England, 1998), p. 715.
[13] M. Kamlah and C. Tsakmakis, Int. J. Solids Struct. **36**, 669 (1999).
[14] Y. Shindo, K. Horiguchi, T. Sugo, and Y. Mano, ASTM J. Test. Eval. **28**, 431 (2001).